# Rapid Interchangeable Hydrogen, Hydride and Proton Species at the Interface of Transition Metal Atom on Oxide Surface

*Simson Wu,[1] Kai-Yu Tseng,[2] Ryuichi Kato,[3] Tai-Sing Wu,[4,5] Alexander Large,[6] Yung-Kang Peng,[7] Weikai Xiang,[8] Huihuang Fang,[1] Jiaying Mo,[1] Ian Wilkinson,[9] Yun-Liang Soo,[4,5] Georg Held,[6] Kazu Suenaga,[3] Tong Li,[8] Hsin-Yi Tiffany Chen[2,*] and Shik Chi Edman Tsang[1*]*

[1]*The Wolfson Catalysis Centre, Department of Chemistry, University of Oxford, Oxford, OX1 3QR, UK*

[2]*Department of Engineering and System Science, National Tsing Hua University, Hsinchu 300044, Taiwan*

[3]*National Institute of Advanced Industrial Science and Technology (AIST), Central 5, 1-1-1 Higashi, Tsukuba 305-8565, Japan*

[4]*National Synchrotron Radiation Research Center, Hsinchu 300, Taiwan*

[5]*Department of Physics, National Tsing Hua University, Hsinchu 300044, Taiwan.*

[6]*University of Reading, Whiteknights, Reading, Berkshire, RG6 6AH, UK*

[7]*City University of Hong Kong, Hong Kong*

[8]*Institute for Materials, Ruhr-Universität Bochum, 44803, Bochum, Germany*

[9]*Siemens plc, CT NTF, Wharf Road, Oxford, OX29 4BP, UK*

*corresponding e-email: edman.tsang@chem.ox.ac.uk*

**ABSTRACT:** Hydrogen spillover is the phenomenon where a hydrogen atom, generated from the dissociative chemisorption of dihydrogen on the surface of a metal species, migrates from the metal to the catalytic support. This phenomenon is regarded as a promising avenue for hydrogen storage yet the atomic mechanism for how the hydrogen atom can be transferred to the support remains controversial for decades. As a result, the development of catalytic support for such purpose is only limited to typical reducible oxide materials. Herein, by using a combination of in-situ spectroscopic and imaging technique, we are able to visualise and observe the atomic pathway for which hydrogen travels via a frustrated lewis pair that has been constructed on a non-reducible metal oxide. The interchangeable status between hydrogen, proton, and hydride is carefully characterised and demonstrated. It is envisaged that this study has opened up new design criteria for hydrogen storage material.

## 1 Introduction:

Reversible hydrogen spillover is a well-recognized phenomenon that has been extensively discussed in solid catalysts and hydrogen storage materials.[1-4] For example, Khoobiar reported that $WO_3$ particle turns to blue $WO_{3-x}$ when it is in contact with a Pt nanoparticle in $H_2$.[5] The blue color appears because hydrogen atoms created by dissociative chemisorption of $H_2$ on Pt, migrate from the Pt surface to the yellow $WO_3$ particles and reduce them to blue $WO_{3-x}$. Such observation can be reversible when $H_2$ is removed from the system. However, the intriguing molecular mechanism how the hydrogen can be reversibly activated from transition metal atom or ion and be migrated to reduce oxide support and in which chemical forms have enormously attracted the attention of many researchers. There is so far no direct visualization on this spillover phenomenon at an atomic level and the interchangeable pathway between gaseous molecular $H_2$, transition metal hydride and proton on refractory oxide support surface is hard to understand by molecular scientists due to complex nature of solid composite catalysts.[6]

On the other hand, since the landmark report from Stephan *et. al.*[7,8] the chemistry of Frustrated Lewis Pair (FLP) has been successfully developed during the last decades in several molecular systems which can reversibly activate $H_2$ heterolytically by the FLP into $H^+$ and $H^-$ and can catalyze hydrogenation of a wide range of substrate

molecules in solvents.[7–11] The frustrated Lewis pair (FLP) is a chemical entity containing both a Lewis acid (LA) and a Lewis base (LB) at sterically hindered positions, which accordingly cannot undergo acid-base adduct formation hence giving them unquenched reactivity. Similarly, recent observation was also made when $H_2$ is dissociated and reversibly activated to protons via FLP mechanism by a redox hydrogenase enzyme containing [FeFe] cofactor in biological system.[8, 12–14] As a result, the formed electrons and $H^+$ from $H_2$ on the redox co-factor are rapidly channelled from the active enzyme. While the former proceeds through electron-conduction via Fe-S bonds, the latter goes through proton-conduction via a proton-transfer pathway (PTP) using compact biological N-ligands (array of proton hopping sites) to enhance ionization and separation of H by $½\ H_2 = H^+ + e^-$ by Le Chatelier's principle.

Herein, we have constructed a precision-engineered Ru atoms supported on the non-reducible MgO(111) surface that can offer unique rationalization of hydrogen activation and migration on solid transition metal-support interface, which provides the important guiding principle and atomic pathway of hydrogen spillover from transition metal atom to oxide support. First, magnesium oxide, which has been vastly employed in catalysis due to ultrahigh chemical stability as well as strong basicity, was selected in this work.[15,16] Also, the unique atomic arrangement of alternated layers of Mg cations and O anions of MgO(111) facet resulting in a net dipole moment and strong electrostatic field and the terminal oxygen anions could help to stabilize and disperse transition metal ions.[17–20] Its high affinity in attracting protons to its surface might provide a driving force for hydrogen migration to occur. By selectively doping Ru on the oxygen terminated surface, we have successfully created a FLP like ion pair between $Ru^{2+}$ and surface $O^{2-}$ in a close proximity sterically separated by O sites directly bonded to the Ru. It is demonstrated by Scanning Transmission Electron Microscopy (STEM), In-situ Ambient Pressure X-ray Photoelectron Spectroscopy (AP-XPS), Operando Fourier-transformed Infra-Red (FTIR), $^1H$ Nuclear Magnetic Resonance (NMR), Atom Probe Tomography (APT) and Density Function Theory (DFT) for the first time that the nature of interfacial Ru is not metallic as that of Ru nanoparticle but as $Ru^{2+}$ due to readily charge transfer to underneath oxygen of the oxide support. Hydrogen can thus be reversibly activated by $Ru^{2+}/O^{2-}$ pair as surface FLP-like ion pair to give $H^-$ and $H^+$. Further redox change triggers the formation of $Ru^o/HO^-$ to convert the $H^-$ to $H^+$. It is therefore exciting to correlate this surface phenomenon for hydrogen migration to the molecular systems/biological evolution systems.

**2 Results and Discussion:**

The preparation of MgO(111) via hydrothermal method and its selective Ru doping is summarized in the supplementary section. Freshly prepared MgO(111) and MgO(110) was characterized by X-ray diffraction (Figure S1) which confirms the nature of periclase magnesium oxide. To ensure the dominant formation of the polar (111) facet, the MgO(111) sample has been dispersed in various solvents and subsequent XRD measurements were carried out[21] (Figure S2). Interestingly, for the ethanol-dispersed sample, it displays a relatively higher intensity of peaks indexed at (111) and (222) reflections and a reduced intensity of the (200) and (220) peaks when compared to the standard non-solvent-dispersed MgO(111) sample. The difference in peak intensity might be attributed to the controlled assembly of the MgO(111) nanosheets for which polar (111) planes are orientated to the same direction with respect to its net dipole moment in the polar solvent. The atomic arrangement of MgO(111), with (111) facet exposed as the top and bottom surface while (220) facet exposed as side planes, facilitate the stacking of the sheets and hence result in the increase in peak intensity of the diffraction patterns. In contrast, when MgO(111) is dispersed in non-polar solvent such as hexane, the non-polar facets are more aligned and hence it shows a relatively higher peak intensity for the (200) and (220) peak.

As shown in Figure S3, bright-field transmission electron microscopy reveals that MgO(111) was made up of hexagonal nanosheets with a size range of 50-200 nm while MgO(110) displays a leaf like structure. The lattice spacing of 0.244 nm for MgO(111) and 0.148 nm for MgO(110) matches well with the literature reports[22,23]. After the immobilization of Ru onto the MgO(111) nanosheets, it can be observed from the high resolution images that the exposed defect free plane is maintained in (111) arrangement without obvious reconstruction (The STEM image in figure S4 show the regular terminal oxygen atoms in 111 arrangement that matches with the expected lattice spacing from corresponding atomic model). In contrast, the exposed plane for Ru/MgO(110) appears to be ill-defined which might be caused by significant charging effect during examination on the structure (Figure S5). Dissimilar to supported Ru nanoparticle in the case of MgO (110) surface, it is worthwhile to note that Ru species remain highly dispersed with plenty of single 'atoms' scattered on surface and occasionally as 2D raft-like structure (no metallic lattice is observed) on defect-free (111) non-reducible MgO (Figure 1a) despite the use of a high concentration of Ru (3.4 weight %, as confirmed by ICP-MS). Single metal 'atom' dispersion on redox-type of oxide supports are commonly reported whereby surface point defects such as oxygen vacancies or step sites with redox metal sites offer stabilization to the metal atoms[24]. In our case, the random sizes of Ru atoms/2D islands suggest a high affinity of this surface for Ru that lead to extensive dispersion on non-reducible and defect-free MgO(111). This is presumably due to the strong surface polarity of the terminated oxygen facet on this oxide surface to stabilize Ru. To analyse the elemental distribution in detail, slices were taken through the Ru/MgO(111) for atomic depth profiling via APT. As displayed in Figure 1b, Ru is indeed dispersed atomically in patches across the MgO surface. Elemental depth concentration profile further reveals that Ru is selectively located over magnesium on the oxygen-terminated surface (Figure 1c)

High angle annular dark field (HAADF) imaging by 60 kV STEM coupled with electron energy loss spectroscopy (EELS) was then performed to examine the precise position of individual Ru 'atomic' sites on the oxygen surface of MgO(111). HAADF-STEM imaging revealed sites scattered across the surface that have a higher contrast than the surrounding top Mg sites (Figure 1d). The Z-contrast nature of HAADF imaging implied that this is due to a heavier constituent atom in the measured spectra. Simultaneous atomic EELS and HAADF acquisitions (Figure 1e and 1f) were performed via a line-scan across a bright contrast dot in Figure 1d. These spectra confirm the presence of Ru atom in the atomic column with the fingerprint Ru $M_{2,3,4,5}$ edges and specifically bonded to the magnesium atoms as evidenced in the elemental mapping (Figure 1f). It is worthwhile to note that the STEM image in Figure 1d was specifically taken from the [110] direction in order to differentiate doping sites due to the striking close resemblance between the simulated STEM images of Ru sitting on the 1-O and 3-O site from the [111] direction (Figure 1g). Interestingly, HAADF-STEM image of the Ru/MgO(111) matches well with the simulation of Ru sitting on the hollow site of 3 oxygen, herein refer to Ru-OOO hollow site, as depicted in Figure 1g. In order to confirm the average coordination environment of the Ru species, x-ray absorption fine structure (EXAFS) was then performed at reaction temperature of 300 $^oC$ for the hydrogen pre-reduced

Ru/MgO(111) sample inside an air-tight cell. It was compelling to observe a significant contribution from Ru-O bond despite extensive hydrogen reduction under 300 °C. Subsequent least square fitting reveals a 3-oxygen coordination to the Ru at 2.03(2)Å with a distance of 3.17(3)Å from underneath Mg (Figure S6), which concomitantly matches with the STEM measurements and our atomic model (Figure 1h). It was exciting to discover the absence of Ru-Ru even at a high Ru loading, which is in contrast to that of the typical 6/7-coordination for Ru nanoparticles. This results in an atomic dispersion that is uniquely offered by the polar oxygen terminated surface of MgO(111). In a nutshell, the EXAFS results for Ru/MgO(111) provide evidence about the atomic Ru-OOO species as the highly disperse Ru on MgO(111) surface. In contrast, the EXAFS spectrum for Ru/MgO(110) only show a 6 coordination Ru-Ru bond without any contribution from Ru-O (Figure S7). In order to further confirm the atomic model, density functional theory computations (DFT) were employed. Single Ru species was placed on different O sites on MgO(111) initially and all the results confirm that the Ru-OOO hollow site atop to Mg is the most stable configuration (Figure S8). On another note, the slight discrepancy between the Ru-O bond length derived from EXAFS and the DFT-optimized model might be attributed to the realistic sample from model morphology as well as contributing thermal factors. The average signal obtained from EXAFS (as a result of a mixture of single atoms and 2D raft-like structure) might lead to a small degree of structural distortion when compared to the single pre-defined structure for the DFT model.

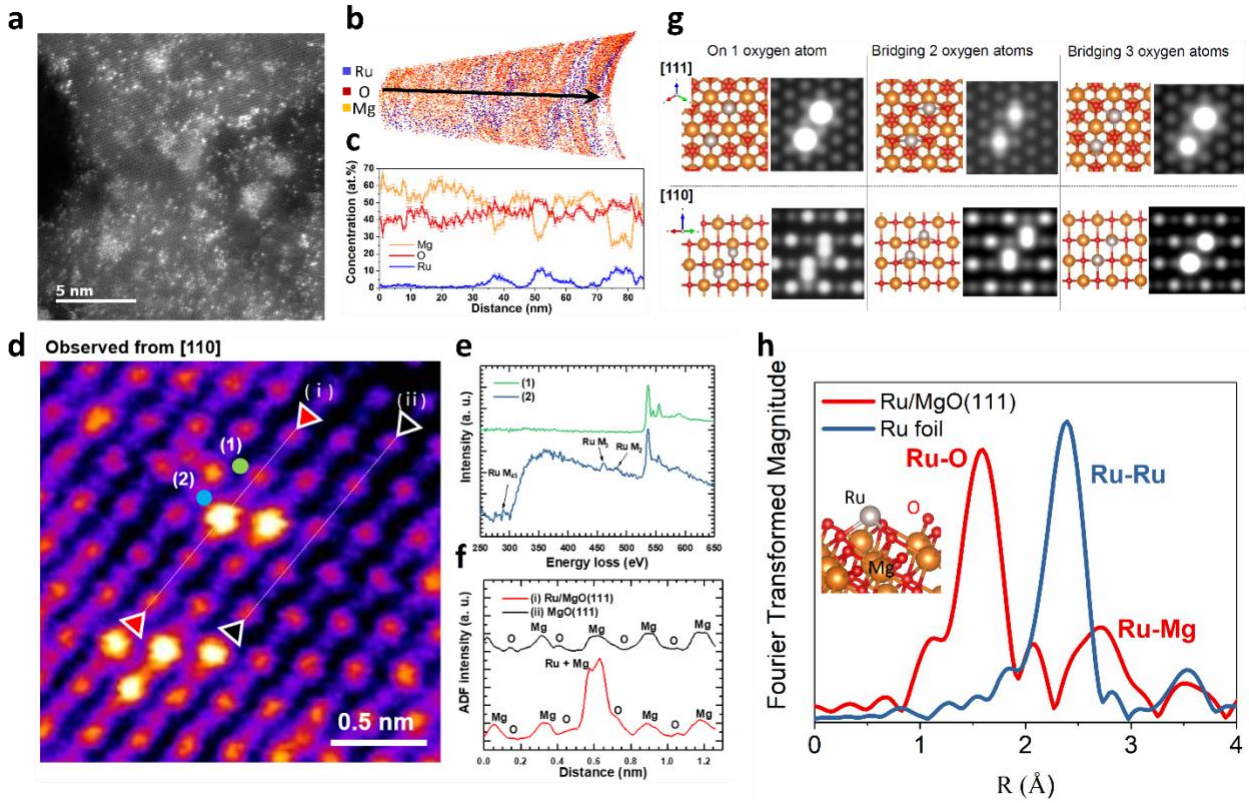


**Figure 1 a** TEM image of 3.4 wt%-Ru/MgO(111) showing 2-D islands and scattered Ru atoms; **b** APT Atom map of 3.4 wt%-Ru/MgO(111), blue: Ru, red: O, orange: Mg; **c** Composition profile of Ru, Mg, O of 3.4 wt%-Ru/MgO(111) along the black line in b; **d** HAADF-STEM image of 3.4 wt%-Ru/MgO(111) observed from [110] direction; **e,f** Simultaneous acquisition **e** EELS extracted on oxygen atom (green circle in **d**), Ru atom (blue circle in **d**) and **f** HAADF acquired along the line in **d**; **g** Simulation of STEM images of 2 Ru atoms supported on different positions of MgO(111) from [111] and [110] direction. Atomic model was also provided for reference; **h** Fourier transform of $k^3$-weighted Ru K-edge of X-ray absorption fine structure spectroscopy (EXAFS) spectra of the post hydrogen-reduced 3.4 wt%-Ru/MgO(111) measured at 300 °C. The Ru metal foil is also included here for reference. Inset shows a simulated model of Ru coordinating with 3-oxygen atoms (trigonal site pointing to underneath Mg) on (111) oxygen terminated surface. White: Ru, orange: Mg, red: O.

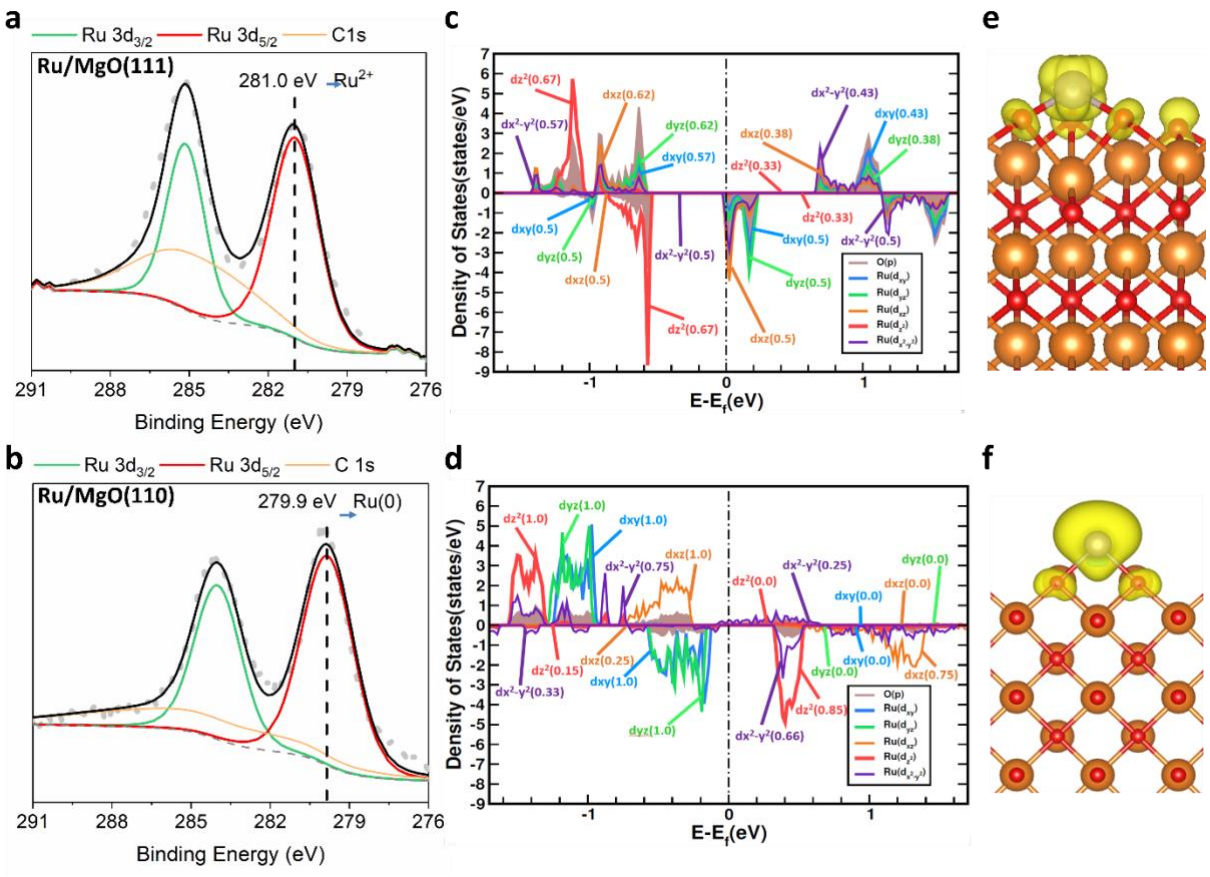


**Figure 2 a,b** Ambient Pressure X-ray Photoelectron Spectroscopy (AP-XPS) Ru 3d spectra for (**a**) Ru/MgO(111) and (**b**) Ru/MgO(110). Measurement was performed under 1 mbar Ar at 350 ºC inside an air-tight sample cell after pretreatment at 1 mbar $H_2$ at 350 ºC. Peak shift was calibrated with reference to the internal standard Mg 2s (88.1 eV)[25], **c,d** Projected Density of States (DOS) of Ru and O for (**c**) Ru/MgO(111) and (**d**) Ru/MgO(110); **e,f** Spin density plots for (**e**) Ru/MgO(111) and (**f**) Ru/MgO(110). Yellow and blue clouds refer to the charge accumulation and depletion respectively. Red spheres: oxygen, orange spheres: magnesium.

To investigate the nature of Ru oxidation state at the atomic interface of Ru/MgO(111), operando near ambient-pressure x-ray photoelectron spectroscopy was performed. The sample was first pre-reduced in flowing hydrogen at 350 $^{o}$C and then switched in-situ to Ar at the same temperature for measurement. Surprisingly, the Ru on MgO(111) showed a positive oxidation state of around +2 whilst Ru on MgO(110) shows a typical metallic state (Figure 2a and 2b). It is noted that Ru was deposited by chemical vapor decomposition of Ru carbonyl and the gas switching from $H_2$ to Ar was carefully performed in a tightly sealed in-situ sample cell without exposure to air. It is thus rather unexpected for its positive oxidation state. In order to ascertain the oxidation state of Ru, in-situ x-ray absorption spectroscopy was further performed at 300 $^{o}$C under flowing He with pre-reduction in hydrogen at the same temperature (Figure S9). Again, it shows a consistently positive oxidation state as evidenced by the shift towards higher binding energy when compared to the Ru(0) metal foil. This can be interpreted as the stabilization of the unstable terminal oxygen surface by Ru at the interface via charge transfer as suggested by Goniakowski *et. al.*[26,27]. Subsequent density of states (DOS) analysis reveals an extensive hybridization between Ru 3d and O 2p orbitals (Figure 2c), leading to the facile hybridization between Ru to the bonded oxygen atoms (Figure 2e). In contrast, for Ru/MgO(110), the Ru 3d and O2p orbitals overlap poorly such that Ru prefers to stay in the metallic state (Figure 2d and 2f). Bader charge analysis was then performed to disseminate the electrostatic charge on the surface Ru and oxygen atoms (Figure S10) via a single Ru atom on MgO(111) model. The DFT results have shed light on the positively charge of about +1.3 of the Ru as similar to the XPS results. Meanwhile, the oxygen atoms directly bonded to the Ru show a reduced charge of -1.1 that might possibly be due to charge quenching. By contrast, the surface oxygen atoms in the close proximity of the Ru-OOO hollow site show a more negative charge of -1.5, herein referred to as $O^{f}$. As a consequence, the surface Lewis acidic nature Ru ion and the Lewis basic $O^{f}$ ions at such atomic interface could possibly form a FLP-like ion pair sterically separated by the hollow site oxygen, which contradicts to the typical structure of Ru nanoparticles (3-D Ru islands) on refractory oxide supports. A schematic depicting the surface charge distribution is displayed in Figure S10b. The close molecular distance between Ru and nearby $O^{f}$ ions could therefore facilitate small molecule activation.

To further access how the [$Ru^{2+}$-$O^{f}$] FLP-like ion pair can facilitate hydrogen activation on the surface, the 3d peaks of Ru as well as the $O_{1s}$ ([OH] composition) peaks were carefully characterized by using AP-XPS, where measurements were carried out by switching the sample feed between reducing ($H_2$) and non-reducing (Ar) gas in operando conditions, see Figure 3a and 3b. To reduce the charging effect and to amplify the kinetics, a higher temperature of 350 $^{o}$C was used to provide a more extensive hydrogen activation and spillover hydrogen. Briefly, the Ru/MgO(111) sample was first heated to 350 $^{o}$C under 1 mbar $H_2$ to remove any surface $RuO_2$ and was then switched back to an Ar atmosphere under the same temperature for the XPS measurement. As agreed with Figure 2a, the Ru on MgO(111) shows an oxidized state of about +2 without being exposed to air under flowing Ar. Meanwhile when the sample feed is switched to hydrogen the Ru(II) is reduced to Ru(0) under the partial pressure of $H_2$ whereas a corresponding increase in the shoulder intensity of the $O_{1s}$ spectrum was observed (Figure 3a and 3b) where the shoulder peak and main peak can be resolved as [OH] and [$O^{2-}$] components, respectively. It's interesting to note a significant increase of OH from 16.4 % to 24.8% for the MgO(111) sample with Ru, indicating that some of hydrogen gas are somehow activated by the transition metal atoms to give protons coverage on surface $O^{2-}$ of MgO(111) surface. This phenomena can be totally reversible once the flowing gas is switched again. It is envisaged that the surface $O^{2-}$ acting as Lewis base donates electron density to the antibonding orbitals of $H_2$ molecule while its bonding electrons interacts with $Ru^{2+}$ as Lewis acid, leading to heterolytic cleavage of $H_2$ to $H^{+}H^{-}$ by the two ion pair. This resembles the nature of the reported homogeneous FLP-like ion pair systems for reversible $H_2$ activation[6]. The hydride nature on Ru-H must then be converted to proton that migrate to the $O^{2-}$ terminated surface of MgO(111) to form $OH^{-}$ while the electron retains to reduce the $Ru^{2+}$ to Ru(0) as observed. In order to confirm the dynamic change of the Ru oxidation state, operando X-ray Absorption Near-Edge Spectroscopy (XANES) was performed at 300 $^{o}$C under switching gas flow (Figure S11). As expected it shows a Ru(0) metallic state under reducing hydrogen atmosphere but swiftly swings to Ru(II) state when the gas flow is switched to He. It thus sheds light on the facile redox transfer in Ru for the interconversion of hydrogenic species. This mechanism differs to typical reducible support (for instance $TiO_2$) that can offer a channel for the duplex pair [H+·e-] to tunnel through via the variable oxidation state of the metal framework of the support[28]. In contrast, for our case of non-reducible support, electrons can only retain in the metal while $H^{+}$ can travel across the $O^{2-}$ surface via proton exchange. Thus, energy is required to separate electrons and protons from activated $H_2$ and channel the protons away from the electrons (against columbic potential). On the other hand, there is no shift in binding energy for Ru 3d nor does shape change in the O1s spectra of Ru/MgO(110) (Figure S12).

In order to further monitor the change of the [OH] on the MgO(111) surface, in-situ Diffuse Reflectance Infra-red Fourier Transform spectroscopy (DRIFT) was performed where the sample feed was switched between nitrogen and hydrogen in operando. The sample was first heated to 250 $^{o}$C under helium to clean the surface which was then cooled down to 200 $^{o}$C for measurement. A blank spectra was recorded at this point. Figure 3c displays the relative absorbance intensity of the difference spectra at 3300 $cm^{-1}$, which is attributed to the [OH] stretching region for Ru/MgO(111). Upon passing nitrogen there was a slight increase in peak intensity presumably due to an inevitable source of water vapor inside the chamber, since this was observed in both the case of Ru/MgO(111) and Ru/MgO(110). However, as it is switched to $H_2$ after 15 minutes, a rapid surge of this peak intensity is observed. This result echoes the in-situ XPS results which demonstrates an increase in the [OH] on MgO(111) upon passing molecular hydrogen. In contrast, the relative change for Ru/MgO(110) was only minimal (Figure S13). The hydrogen species on MgO(111) and Ru-MgO(111) were also monitored by static $^{1}$H solid state NMR in Ar at room temperature upon their pre-reduction in $H_2$ at 350$^{o}$C. Figure 3d shows the two signals of 0.71ppm (extensive hydroxyl surface with H-bonding) and 5.43 ppm (isolated -OH) of typical hydroxylated MgO(111)[29]. For the Ru-doped MgO(111), we can still see the ruminant hydride nature of Ru-H with a major peak at -1.7 ppm attributed to Ru-H on polar MgO(111) and trace peak at -4.8ppm to more hydridic Ru-H probably associated with contaminated non-polar MgO in background of 0.75 ppm of extensive hydroxyl surface on MgO(111).

To correlate the atomic locations of $Ru^{2+}$ for hydrogen activation with the locations for proton formation at the Ru-MgO (111) interface, APT has been employed to directly visualize the elemental distribution of Ru/MgO(111) after hydrogen pre-treatment at 350 $^{o}$C. Note that a high temperature reduction was also used in order to enhance the kinetics and hence amplified the

hydrogen spillover effects. Although H is in principle can be monitored by the precision pixilated mass spectroscopy in the APT equipment, the errors can be significant due to indiscriminative adsorption and accumulation of H-containing residue gas to the sample surface in the vacuum chamber. Figure 3e and 3f display the APT spectra after the hydrogen-dosed Ru/MgO(111) that shows the close resemblance of the atomic distribution of hydroxyl groups (at 17 Da in the mass spectrum) to the locations of Ru as the original source of spillover H. The concentration of OH is consistently higher than that of Ru with some regions for spillover (protonic species is residing on the oxygen surface of MgO(111) instead of Ru locations), presumably due to the hopping of protons on the $O^{2-}$ covered surface. The surface OH groups can be considered as fingerprint for the activation and migration of protons on $O^{2-}$ from Ru-H sites to the close proximity of oxygen terminated surface sites since it is shown to be kinetically unfavorable for the MgO(111) itself to dissociate hydrogen molecule. In contrast, a low concentration of [OH] was observed before hydrogen dosage which might be possibly due to the residual hydrogen atoms during synthesis or water molecules in ambient moisture environment (Figure S14a). The isosurface map in Figure S15 also sheds light on the vast distribution of hydrogen as [OH] on the MgO surface.

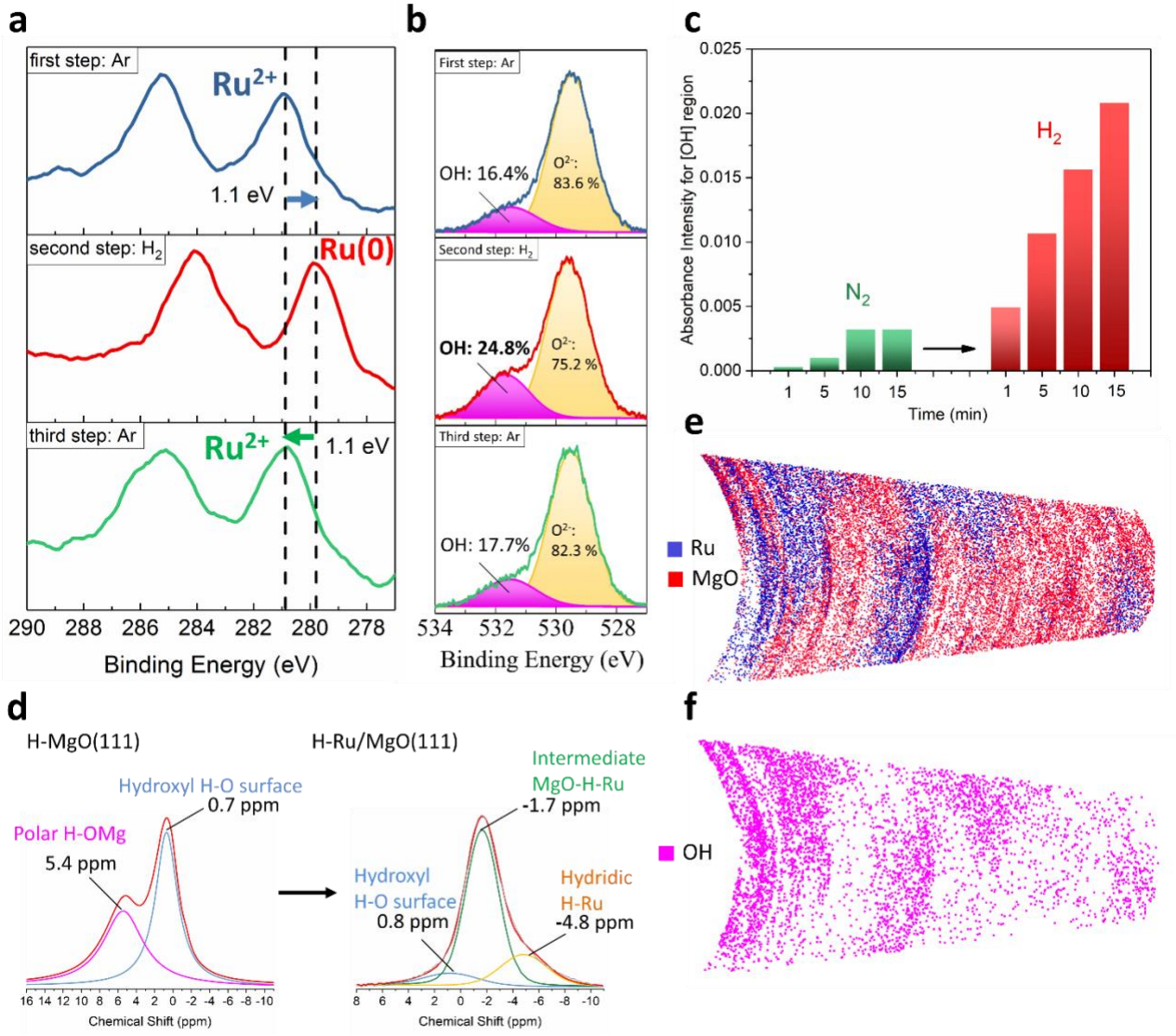


**Figure 3** **a** Ru 3d and **b** O1s of AP-XPS spectra at 350 °C under alternative sweeping between 1 mbar Ar and 1 mbar $H_2$; **c** In-situ FTIR under 1 bar of $N_2$ and $H_2$ at 200 °C; **d** $^1$H NMR spectra of MgO(111) and Ru/MgO(111) after $H_2$ reduction; **e,f** Atomic probe tomography (APT) of Ru/MgO(111) after passing hydrogen at 350 °C. 3D atomic mapping of surface atomic distribution of **e** Ru and MgO (Blue: Ru, Red: MgO); **f** OH (Pink: OH).

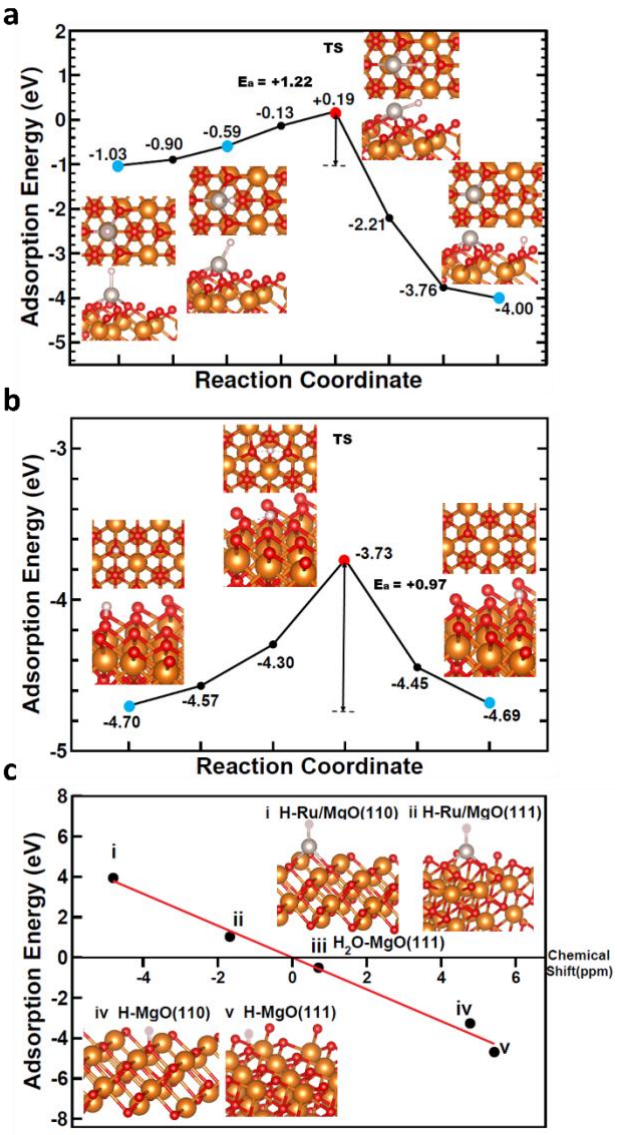


**Figure 4 a** Calculated energy profile with optimized structures of hydrogen transfer from Ru-H to proton on $O^{2-}$ of MgO(111); **b** Calculated energy profile for proton migration from terminal O sites on MgO(111), H transfer energy = -3 eV from Ru-H to $O^{2-}H^{+}$ on MgO(111) showing the thermodynamic favored protonation of the polar MgO(111) and surface proton hopping energy = 0.01 eV. Climbing-Image Nudged elastic band (CI-NEB) was used. All H absorption energies are normalized to the energy of an isolated hydrogen molecule in gas phase; **c** Linear relationship between experimental observed $^{1}$H-NMR chemical shift and computed proton absolute magnitude of absorption energy by density function theory: i. atop H on Ru supported on MgO(110); ii. atop H on Ru supported on MgO(111); iii. Hydrated/hydroxylated on MgO; iv. atop H on oxygen atom of MgO(110); v. atop H on oxygen atom of MgO(111). Negative sign of adsorption energy indicates electron withdrawing to form protonic species and positive sign for electron donating to form hydridic species. Red sphere: oxygen, orange sphere: magnesium.

To verify the mechanism of hydrogen activation and spillover from Ru to the oxygen terminated surface of MgO(111) and the proton hopping across the oxygen sites of MgO(111), DFT calculations were employed to show spontaneous movements of the hydrogen (Figure 4A and 4B). The ultra-stability for proton to adsorb on the highly energetic oxygen terminated surface of MgO(111) facet (-4 eV relative to an isolated hydrogen molecule, and -3 eV reaction energy (the energy difference between the reactant and product)) with respect to the difference between the final state and initial state) gives the strong thermodynamic driving force to provide a labile migration from the metal-hydride surface to the polar oxide support surface. The transfer of the hydrogen from the atop site on Ru to a transition state adjacent to the nearby atop oxygen site has an activation energy of 1.22 eV and can be as low as 0.32 eV (+0.19-(-0.13)) if the initial position begins at the close proximity of the oxygen site (driven by the charge deficient polar surface). On the other hand, the hopping of hydrogen (more precisely proton) across adjacent surface oxygen sites, has an activation energy that varies from 0.57 to 0.97 eV. The lower proton hopping energy barrier relative to the spillover energy barrier ensures the readily availability of the oxygen sites near Ru from surface diffusion such that a fast and continuous hydrogen spillover is ensured.

Figure 4c shows the correlation of $^{1}$H NMR signals from the different nature of hydrogenic species measured with their absolute quantity of adsorption energy derived from DFT calculations. As implied from the calculations, the nature of H as in whether the H is hydridic, neutral or protonic from chemical shift value is highly dependent on electronic affinity of structures underneath to form stable compound in a linear relationship[30] as shown in the Figure 4c. For example, H on $Ru^{2+}$ over MgO(111) gives lower adsorption energy than that of H on Ru(0) over MgO(110), and hence less hydridic character associated with lower chemical shift is observed (see Fig. 3d); whereas stronger adsorption energy to give protonic nature of hydrogen over MgO(111) than MgO(110) is also obtained. As a result, this provides the atomic pathway for the interconversion between hydride and proton such that the latter can migrate to the oxygen surface while the electron will be retained at $Ru^{+2}$ and reduce it to Ru(0) state. This mechanism agrees well with the in-situ AP-XPS and FTIR result for the observation of reduction of Ru(II) to Ru(0) with a concomitant increase in [OH].

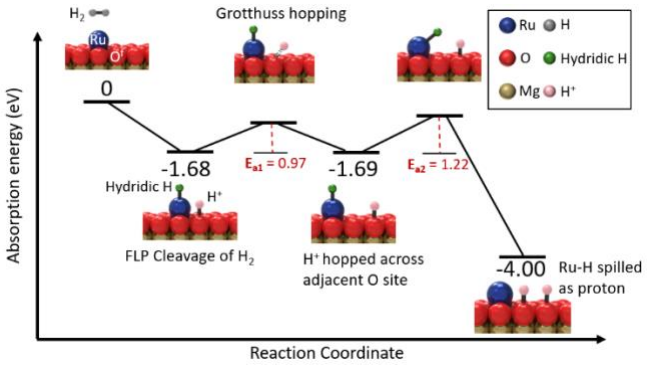


**Figure 5.** Proposed mechanism from left to right: dissociative dihydrogen activation on $Ru^{2+}/O^{2-}$ FLP like ion pair to give $H^{-}$ and $H^{+}$; facile first $H^{+}$ hopping between surface oxygen sites to create vacancy site on MgO(111) induces redox conversion of $H^{-}$ from Ru-H to give $Ru^{0}$ and second $H^{+}$. The value of energy change comes from corresponding DFT calculations and is thermodynamic driven on polar MgO (111).

According to the proposed mechanism in Figure 5, a reversible reaction pathway for facile hydrogen activation by interfacial Ru and hydrogen spillover on a non-reducible polar oxide support with backing from the experimental techniques (STEM, APT, AP-XPS, FTIR and NMR) and DFT calculations is for the first time provided. As $H_2$ approaches the surface, the Frustrated Lewis Pair (FLP)-like interfacial Ru(II) and surface oxygen ($O^{2-}$) at the metal-oxide interface offers the thermodynamic driving force for $H_2$ activation, redox transfer of Ru-hydride to proton on $O^{2-}$ at the metal-support interface, followed by Grotthuss hopping mechanism from surface diffusion on the oxygen terminated polar surface with low activation barrier for their readily spillover. This pathway could temperamentally reduce the dynamic coverage of hydrogenic species from Ru or $O^{2-}$, allowing adsorption and catalysis of substrate molecule for higher rate of hydrogenation or dehydrogenation at their competitive partial pressures with respect to hydrogen gas. For example, we have previously shown that Ru/MgO(111) can effectively promote ammonia synthesis at higher rate at elevated temperature by alleviating hydrogen poisoning on Ru surface under dynamic conditions.[29] It is envisaged for conventional transition metal nanoparticle on refractory oxide support systems, the non-metallic nature of interfacial metal species on oxide surface with particular facets may still play an important part from those classical adsorbed H atoms migration on Ru nanoparticle to oxide surface[4-6]. The interrelationships with hydride at interface and proton on refractory oxide surface may warranty further studies.

**3 Conclusions:**

To summarize, it is demonstrated a facile reversible hydrogen spillover atomic pathway on a polar MgO(111) support is facilitated by a Frustrated Lewis Pair like ion pair between Ru(II) and $O^{2-}$ at the metal-support interface. APT has provided direct visualization of the H (in form of hydroxyl groups) on the MgO(111) surface whereas in-situ XPS and DRIFT shed light on the mechanism for $H_{ads}$ atoms to migrate from the Ru surface to the $O^{2-}$ surface which otherwise doesn't possess the ability to dissociate $H_2$ molecule. We envisage this study can provide insights into designing more efficient hydrogenation, dehydrogenation and hydrogenolysis type of catalysts using a wider range of oxide supports that can excel in hydrogen spillover applications.

## AUTHOR INFORMATION


### Corresponding Author

edman.tsang@chem.ox.ac.uk


### Notes

The authors declare no competing financial interest.

## SUPPORTING INFORMATION

Supporting Information is included, ending with "This material is available free of charge via the Internet at http://pubs.acs.org."

- Experimental procedures; supplementary figures

## ACKNOWLEDGMENT


The financial support of this work from the EPSRC research council of UK and Siemens, plc are acknowledged. SW thanks to Siemens, plc and EPSRC for a joint DPhil Studentship and YKP acknowledges a Clarendon DPhil Scholarship at the Oxford University, UK. The authors also acknowledge the use of STEM facilities of National Institute of Advanced Industrial Science and Technology of Japan; the use of AP-XPS facilities in the beamline B07 of Diamond Light Source, UK and the use of XAS facilities of National Synchrotron Radiation Research Center, Taiwan. WX and TL thank Deutsche Forschungsgemeinsschaft (DFG) for financial support (project number 407513992) and Zentrumfür Grenzflächendominierte Höchstleistungswerkstoffe (ZGH) at Ruhr University Bochum for the access to infrastructure (FEI Helios G4 CX FIB/SEM and Cameca LEAP 5000 XR).


## REFERENCES


(1) Im, J.; Shin, H.; Jang, H.; Kim, H.; Choi, M. Maximizing the Catalytic Function of Hydrogen Spillover in Platinum-Encapsulated Aluminosilicates with Controlled Nanostructures. *Nat. Commun.* **2014**, *5*, 3370.

(2) Prins, R. Hydrogen Spillover. Facts and Fiction. *Chem. Rev.* **2012**, *112*, 2714–2738.

(3) Broom, D. P.; Hirscher, M. Irreproducibility in Hydrogen Storage Material Research. *Energy and Environmental Science*. Royal Society of Chemistry November 1, 2016, pp 3368–3380.

(4) Bettahar, M. M. The Hydrogen Spillover Effect. A Misunderstanding Story. *Catal. Rev. - Sci. Eng.* **2020**, 1–39.

(5) Khoobiar, S. Particle to Particle Migration of Hydrogen Atoms on Platinum-Alumina Catalysts from Particle to Neighboring Particles. *Journal of Physical Chemistry*. American Chemical Society 1964, pp 411–412.

(6) Karim, W.; Spreafico, C.; Kleibert, A.; Gobrecht, J.; VandeVondele, J.; Ekinci, Y.; van Bokhoven, J. A. Catalyst Support Effects on Hydrogen Spillover. *Nature* **2017**, *541*, 68–71.

(7) Welch, G. C.; San Juan, R. R.; Masuda, J. D.; Stephan, D. W. Reversible, Metal-Free Hydrogen Activation. *Science* **2006**, *314*, 1124–1126.

(8) Stephan, D. W. The Broadening Reach of Frustrated Lewis Pair Chemistry. *Science* **2016**, *354*, 7229.

(9) Chase, P. A.; Welch, G. C.; Jurca, T.; Stephan, D. W. Metal-Free Catalytic Hydrogenation. *Angew. Chem. Int. Ed.* **2007**, *46*, 8050–8053.

(10) Paradies, J. Metal-Free Hydrogenation of Unsaturated Hydrocarbons Employing Molecular Hydrogen. *Angew. Chem. Int. Ed.* Wiley-VCH Verlag April 1, 2014, pp 3552–3557.

(11) Mahdi, T.; Stephan, D. W. Facile Protocol for Catalytic Frustrated Lewis Pair Hydrogenation and Reductive Deoxygenation of Ketones and Aldehydes. *Angew. Chemie - Int. Ed.* **2015**, *54*, 8511–8514.

(12) Tutusaus, O.; Ni, C.; Szymczak, N. K. A Transition Metal Lewis Acid/Base Triad System for Cooperative Substrate Binding. *J. Am. Chem. Soc.* **2013**, *135*, 3403–3406.

(13) Winkler, M.; Senger, M.; Duan, J.; Esselborn, J.; Wittkamp, F.; Hofmann, E.; Apfel, U. P.; Stripp, S. T.; Happe, T. Accumulating the Hydride State in the Catalytic Cycle of [FeFe]-Hydrogenases. *Nat. Commun.* **2017**, *8*, 1–7.

(14) Kalz, K. F.; Brinkmeier, A.; Dechert, S.; Mata, R. A.; Meyer, F. Functional Model for the [Fe] Hydrogenase Inspired by the Frustrated Lewis Pair Concept. *J. Am. Chem. Soc.* **2014**, *136*,

16626–16634.
(15) Mutch, G. A.; Shulda, S.; Mccue, A. J.; Menart, M. J.; Ciobanu, C. V; Ngo, C.; Anderson, J. A.; Richards, R. M.; Vega-Maza, D. Carbon Capture by Metal Oxides: Unleashing the Potential of the (111) Facet. *J. Am. Chem. Soc.* **2018**, *140*, 4736–4742.
(16) Hu, J.; Song, Z.; Chen, L.; Yang, H.; Li, J.; Richards, R. Adsorption Properties of MgO(111) Nanoplates for the Dye Pollutants from Wastewater. *J. Chem. Eng. Data* **2010**, *55*, 3742–3748.
(17) Hacquart, R.; Jupille, J. Hydrated MgO Smoke Crystals from Cubes to Octahedra. *Chem. Phys. Lett.* **2007**, *439*, 91–94.
(18) Finocchi, F.; Goniakowski, J. The Effects of Exchange and Correlation on the Computed Equilibrium Shapes of Wet MgO Crystallites. *Surf. Sci.* **2007**, *601*, 4144–4148.
(19) Geysermans, P.; Finocchi, F.; Goniakowski, J.; Hacquart, R.; Jupille, J. Combination of (100), (110) and (111) Facets in MgO Crystals Shapes from Dry to Wet Environment. *Phys. Chem. Chem. Phys.* **2009**, *11*, 2228.
(20) Pojani, A.; Finocchi, F.; Goniakowski, J.; Noguera, C. A Theoretical Study of the Stability and Electronic Structure of the Polar 111 Face of MgO. *Surf. Sci.* **1997**, *387*, 354–370.
(21) Tang, M.; Ren, Y.; Hu, Y.; Ye, L.; Yue, B.; He, H. Synthesis and Orientational Assemblies of MgO Nanosheets with Exposed (111) Facets. *Chinese Chem. Lett.* **2018**, *29*, 935–938.
(22) Wang, F.; Ta, N.; Shen, W. MgO Nanosheets, Nanodisks, and Nanofibers for the Meerwein–Ponndorf–Verley Reaction. *Appl. Catal. A Gen.* **2014**, *475*, 76–81.
(23) Chen, J.; Tian, S.; Lu, J.; Xiong, Y. Catalytic Performance of MgO with Different Exposed Crystal Facets towards the Ozonation of 4-Chlorophenol. *Appl. Catal. A Gen.* **2015**, *506*, 118–125.
(24) Liu, J. C.; Wang, Y. G.; Li, J. Toward Rational Design of Oxide-Supported Single-Atom Catalysts: Atomic Dispersion of Gold on Ceria. *J. Am. Chem. Soc.* **2017**, *139*, 6190–6199.
(25) Larichev, Y. V.; Moroz, B. L.; Prosvirin, I. P.; Likholobov, V. A.; Bukhtiyarov, V. I. XPS Study of Metal-Support Interaction in Ru/MgO Catalyst for Low-Temperature Ammonia Synthesis. *Chem. Sustain. Dev.* **2003**, 11, 155-160.
(26) Vervisch, W.; Mottet, C.; Goniakowski, J. Theoretical Study of the Atomic Structure of Pd Nanoclusters Deposited on a MgO(100) Surface. *Phys. Rev. B* **2002**, *65*, 245411.
(27) Goniakowski, J.; Noguera, C. Characteristics of Pd Deposition on the MgO(111) Surface. *Phys. Rev. B* **1999**, *60*, 16120–16128.
(28) Panayotov, D. A.; Burrows, S. P.; Yates, J. T.; Morris, J. R. Mechanistic Studies of Hydrogen Dissociation and Spillover on Au/TiO $_2$: IR Spectroscopy of Coadsorbed CO and H-Donated Electrons. *J. Phys. Chem. C* **2011**, *115*, 22400–22408.
(29) Wu, S.; Peng, Y.-K.; Chen, T.-Y.; Mo, J.; Large, A.; McPherson, I.; Chou, H.-L.; Wilkinson, I.; Venturini, F.; Grinter, D.; Ferrer Escorihuela, P.; Held, G.; Tsang, S. C. E. Removal of Hydrogen Poisoning by Electrostatically Polar MgO Support for Low-Pressure NH 3 Synthesis at a High Rate over the Ru Catalyst . *ACS Catal.* **2020**, *10*, 5614–5622.
(30) Jameson, C. J. UNDERSTANDING NMR CHEMICAL SHIFTS. *Annu. Rev. Phys. Chem.* **1996**, *47*, 135–169.

## Table of Contents artwork